Prêt entre bibliothèques - Document expédié

No emprunteur

Expédié via: WebPDF

Adresse: Interlibrary Loans, LB-331
Concordia University Webster Library
1455 De Maisonneuve Boul. W
Montreal, QC
Canada H3G 1M8

Téléphone: (514) 848-2424 **Télécopie:** (514) 848-2801
FTP: 132.205.102.24 **Courriel:** lib-InterLibraryLoans@concordia.ca

De: Prêt entre bibliothèques
Université Laval, Bibliothèque scientifique, Pavillon Alexandre-Vachon, Local 0025
1045 avenue de la Médecine
Québec QC G1V 0A6

Téléphone: (418) 656-2131 **Télécopie:** (418) 656-7699
FTP: 132.203.85.26 **Courriel:** colombo.peb.sciences@bibl.ulaval.ca
Fournisseur: QQLAS

Demande: QMG 868095 **Dem reçue:** 29-JUN-2015
Notre No réf: 1654643 **Expédié:** 30-JUN-2015
Titre: Journal of nanoscience and nanotechnology.

Titre article: Ferromagnetism in Annealed Ce0.95Co0.05O2and Ce0.95Ni0.05O2 Nanoparticles.
Auteur article: S. K. Misra, S. I. Andronenko, J. D. Harris, A. Thurber, G. L. Beausoleil II
Volume/Numéro: v. 13, issue. 10 **Date:** 2013 **Pages:** 6798 - 6805
Nombre d'unités: 8 **Frais:** .00 CAD
Assuré: CAD

[ ] Signature usager requise **[ ] Reproduction interdite** **[ ] Consultation sur place** **[ ] Utilisation supervisée**

Notes:

CECI N'EST PAS UNE FACTURE/THIS IS NOT AN INVOICE

Journal of
Nanoscience and Nanotechnology
Vol. 13, 6798–6805, 2013

RESEARCH ARTICLE

Ferromagnetism in Annealed $Ce_{0.95}Co_{0.05}O_2$ and $Ce_{0.95}Ni_{0.05}O_2$ Nanoparticles

S. K. Misra[1,*], S. I. Andronenko[2], J. D. Harris[3], A. Thurber[4], G. L. Beausoleil II[4], and A. Punnoose[4]

[1] *Department of Physics, Concordia University, 1455 de Maisonneuve Boulevard West, Montreal, QC H3G 1M8, Canada*
[2] *Institute of Physics, Kazan Federal University, Kremlevskaya, 18, 420008, Kazan, Russian Federation*
[3] *Department of Chemistry, Northwest Nazarene University, Nampa, Idaho 83686, USA*
[4] *Department of Physics, Boise State University, Boise, Idaho 83725, USA*

This paper reports an investigation on the role of transition-metal ions in producing ferromagnetism in CeO_2 nanoparticles by electron paramagnetic resonance (EPR). Several samples of CeO_2 nanoparticles annealed at 200, 300, 400, and 500 °C, doped with 5% Ni and 5% Co ions, characterized by X-ray diffraction (XRD), X-ray photoelectron spectroscopy (XPS), thermogravimetry analysis (TGA) and mass spectroscopy (MS), were investigated by *X*-band EPR at 4, 10 and 300 K, and by magnetometry at 300 K. Magnetic properties and EPR/FMR (Ferromagnetic Resonance) spectra of these nanoparticle samples were found to depend strongly on the annealing temperature (T_A), oxygen stoichiometry, and dopant-ion species. Different behavior of saturation magnetization in the samples with the dopants, Co and Ni, is found to be due to different—inward and outward—surface diffusion of these impurity ions, respectively, during annealing. A detailed simulation of EPR/FMR spectra of isolated Co and Ni ions carried out here provides in-depth details on the role of the doped ions and oxygen (O^-) defects played in the observed magnetic properties.

Keywords: CeO_2 Nanoparticles, Spectroscopy, Ferromagnetism, Magnetic Properties.

1. INTRODUCTION

Many efforts were made in recent decade to the investigations different kinds of magnetic nanoparticles.[1] In particular, recent studies have shown that doping with transition-metal (TM) ions produces room-temperature ferromagnetism in ceria (CeO_2), suggesting that this material has the potential for use in spintronic devices. Ni^{2-4} and Co^{5-15} ions have been the most commonly exploited TM ions to produce ferromagnetism in CeO_2. The Co^{2+} ion has a larger magnetic moment with $\mu_{eff} = 4.8\ \mu_B$ compared to $\mu_{eff} = 1.9\ \mu_B$ for the Ni^{2+} ion. This paper reports a detailed investigation of the magnetic properties by EPR spectroscopy and magnetometry of ceria nanoparticles doped with 5% Ni ions, and 5% Co ions and annealed at temperatures in the 200 to 500 °C range. This study unravels the roles played by annealing temperature and oxygen stoichiometry.

*Author to whom correspondence should be addressed.

2. EXPERIMENTAL: SYNTHESIS AND MEASUREMENT

The samples were synthesized by co-precipitation of appropriate concentrations of Ce(III) acetate and either Ni(II) acetate or Co(II) acetate in a lithium hydroxide solution of denatured ethanol. Details of the synthesis and characterization studies using XRD, TEM, XPS and magnetometry have been reported elsewhere.[2,3] Annealing was accomplished under flowing nitrogen at temperatures of 200, 300, 400 and 500 °C for 30 minutes each. Thermal processing was preformed in a nitrogen environment with ramp rates of 20–50 °C/min from 50 °C to 1000 °C. Chemical species released from the sample, phase changes and weight loss as a function of temperature were characterized using a Mettler Toledo TGA/DSC1 thermal analyzer, connected to a Pfieffer Vacuum ThermoStar mass spectrometer. EPR data were recorded at 10 and 300 K on a Bruker X-band ELEXSYS E500 spectrometer.

1533-4880/2013/13/6798/008 doi:10.1166/jnn.2013.7778

3. DISCUSSION OF EXPERIMENTAL DATA

3.1. X-Ray Diffraction and Thermogravimetry-Mass Spectrometry (TGA-MS) Analysis

Powder X-ray Diffraction pattern, shown in Figure 1(a), indicates only a pure ceria phase; no new peaks were observed when annealed at any temperature, thus ruling out any chemical phase changes. The crystallinity improved, whereas the peak width narrowed, with increasing annealing temperatures. Analysis of peak widths showed that the crystallite size increased from ~2.7 nm for the sample annealed at 200 °C to ~4.9 nm for the sample annealed at 500 °C. The TGA-MS data of undoped ceria, in conjunction with the differential scanning calorimetry data, shown in Figure 2, do not indicate any major chemical or structural phase change due to the variations in annealing temperatures. Weak features observed in the TGA data over 50–150 °C and 200–400 °C ranges can be attributed to the release of water and organic species from the acetates (Fig. 2), based on the MS data. The MS data also indicates a steady loss of oxygen (Fig. 2) at temperatures above 300 °C. The Ni- and Co-doped ceria samples displayed similar behavior, as indicated by the TGA-MS data.

3.2. XPS Spectra and Magnetization Measurements

XPS spectra displayed no changes in the chemical state of Ni or Co as a result of annealing. The Ni surface concentration increased as a result of annealing, while the Co concentration decreased. This behavior indicates a tendency of the dopant ions to diffuse during annealing, outward for Ni and inward for Co. Magnetization curves, shown in Figures 1(b) and (c), demonstrate that the annealed samples have a much higher magnetization than the as-prepared samples. While all the Co-doped samples annealed in the 200–500 °C temperature range and Ni doped samples annealed at temperatures < 400 °C showed ferromagnetism with well-defined coercivity, the 500 °C-annealed Ni-doped ceria did not

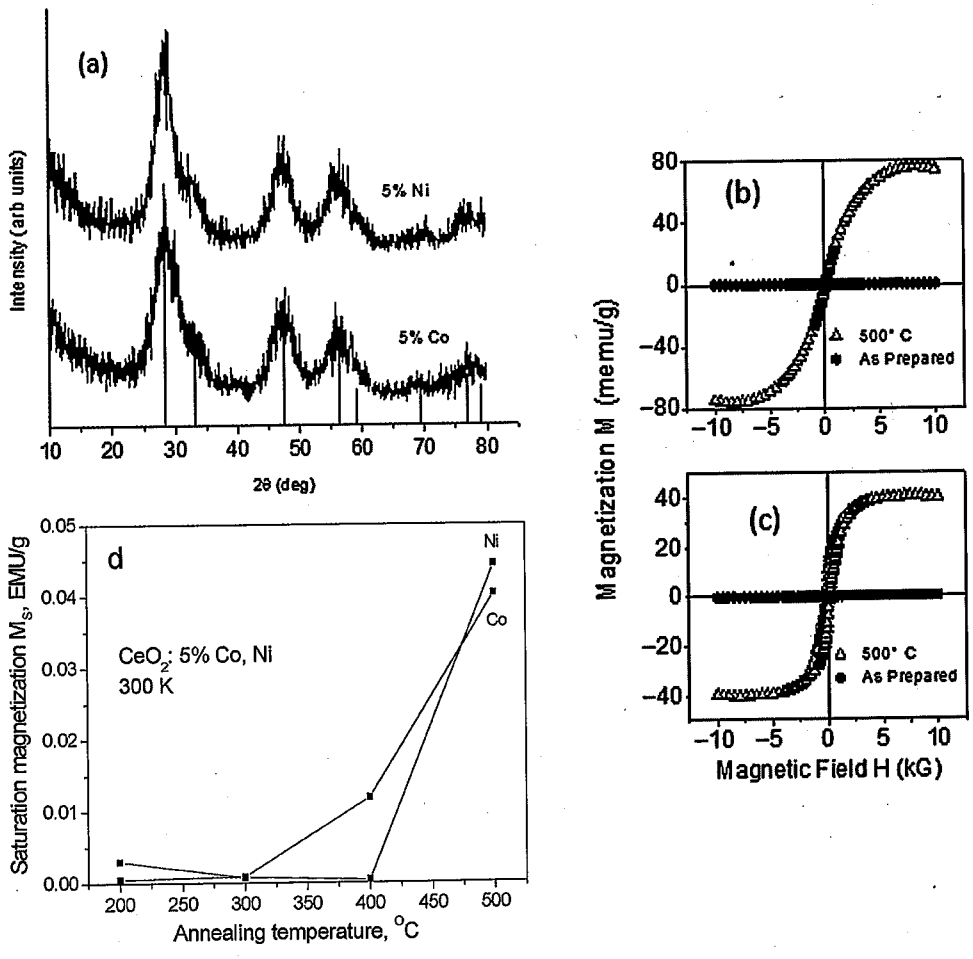

Fig. 1. (a) X-ray diffraction patterns of 5% Ni doped CeO_2 and 5% Co doped CeO_2 nanoparticles for as-prepared and annealed (T_A) at 500 °C samples. Vertical lines show expected positions and relative intensities of CeO_2; (b) M versus H curve of 5% Ni doped CeO_2 nanoparticles collected from as-prepared samples and after annealing at 500 °C for 30 minutes; (c) M versus H curve of 5% Co doped CeO_2 nanoparticles collected from as-prepared samples and after annealing at 500 °C for 30 minutes; (d) Saturation magnetization versus annealing temperature for 5% Ni-doped CeO_2 and 5% Co-doped CeO_2 nanoparticles.

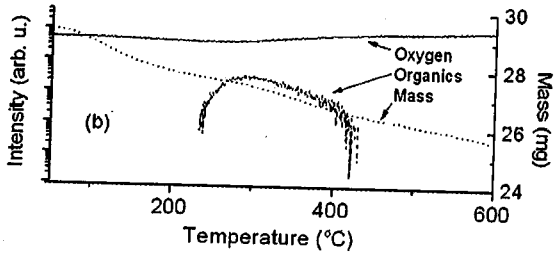

Fig. 2. Thermogravimetry data showing the mass change with temperature (labeled mass), and mass spectroscopy data showing the release of selected organic groups (labeled organics) and oxygen molecules (labeled oxygen) from CeO_2 nanoparticles.

show a measurable coercivity, indicating superparamagnetic behavior. Magnetization results are listed in Table I for both Co and Ni doped CeO_2, showing that the Co-doped samples become progressively more ferromagnetic, while the Ni doped samples become more superparamagnetic with increased annealing temperature. Saturation magnetization of 5% Ni and 5% Co doped CeO_2 are shown in Figure 1(d).

3.3. EPR/FMR Measurements

Spectra at 10 K. (a) Ni. EPR signals due to isolated Ni^{2+} ions (spin $S = 1$) were observed in the samples annealed at 200 °C, similar to those reported by Misra et al.[16] in Ni doped CeO_2 samples at 5 K. On the other hand, the spectra changed in the samples annealed at 300° and 400 °C; a ferromagnetic (FM) line appeared, along with sharp EPR lines due to Ni^+, or Ni^{3+}, ions, the latter characterized by the spin $S = 1/2$ (see Fig. 3(a)). As well, an intense narrow line, characterized by $g \sim 2.0$, due to O^- defects was observed. In the sample annealed at 500 °C, only a strong FM line was observed. The simulated spectrum is shown in Figure 3(a), showing a very good agreement with the experimental spectrum for magnetic field values below 3500 G. However, it was not possible to identify the magnetic species to which belong the EPR spectra above 4000 G. *(b) Co.* EPR spectra due to isolated Co^{2+} ions, observed in all samples, are shown in Figure 3(b). A different Co spectrum, associated with a peak near $g = 4.8$, was exhibited by the samples annealed at 400 and 500 °C. FMR lines were observed in all these samples. The simulation of EPR spectrum shown in Figure 4(b) displays an excellent agreement with the observed spectrum. The EPR data indicate that the local environment around Ni or Co changes systematically with the annealing temperature, T_A, presumably due to the continuous oxygen loss, as exhibited by the TGA-MS data shown in Figure 2. The 10 K EPR spectra in CeO_2, synthesized at 650 °C and treated in a different atmosphere, as reported by Colis et al.[15] are similar to those in the sample annealed at 500 °C, investigated in the present work (Fig. 3(b)). However, the broad EPR signal at $g = 4.8$, assigned to inhomogeneous isolated Co distribution, is similar to that in $Zn_{0.9}Co_{0.1}O$ thin films.[17]

EPR Spectra at 300 K. (a) Ni. No sample displayed spectra of isolated Ni ions at 300 K (see Fig. 3(c)). Simulation of these EPR spectra revealed the presence of both ferromagnetic and superparamagnetic contributions, in accordance with the magnetization measurements. The EPR spectrum of the superparamagnetic part exhibits a symmetric signal centered at $g = 2.0$, whereas the ferromagnetic part of the signal is situated at $g > 2.0$. Accordingly, in the samples annealed at 500 °C, the superparamagnetic part is found to be about 95%, with the spectrum being an overlap of EPR lines with different linewidths from 400 to 3000 G, at the observed value of $g_Z = 2.2$, which is similar to that, observed for CeO_2 samples doped with more than 4% Ni, as reported by Misra et al.[16] Simulation of EPR spectra of the samples annealed at 300 °C revealed that the superparamagnetic component is about 15% and the ferromagnetic component is about 85%, as evidenced by the integrated area of the corresponding lines. The EPR line observed in the sample annealed at 400 °C shows a complex nature: it consists of a superparamagnetic part, and two other lines, presumably ferromagnetic, with contributions of 23% and 64%, as estimated by simulation of this line to be an overlap of two lines with appropriate integrated intensity. There is some evidence of the presence of a very weak FM line in the sample annealed at 200 °C. There is also observed a very intense EPR line at $g = 2.004$, the same as that observed in CeO_2.[16] It is most likely that this line belongs to an oxygen vacancy.[18] It is absent in the samples annealed at 200 and 500 °C, but it is present with a rather low intensity in the sample annealed at 300 °C, and achieves its maximum intensity in the sample annealed at 400 °C. It is noted in this context that the magnetization of the samples annealed at 200, 300, and

Table I. Magnetic properties of CeO_2, doped with Ni or Co, measured at 300 K.

	5% Co:CeO_2			5% Ni:CeO_2	
Annealing temperature T_A (°C)	Average size from XRD L (nm)	Saturation magnetization M_s (emu/g)	Description	Saturation magnetization M_s (emu/g)	Description
200	2.7±0.7	4.56$E-4$	Weakly ferromagnetic	0.00293	Weakly ferromagnetic
300	3.5±1.8	8.25$E-4$	Weakly ferromagnetic	6.99E-4	Weakly ferromagnetic
400	3.7±1.4	0.0118	Ferromagnetic	3.61E-4	Weakly ferromagnetic
500	4.9±1.3	0.0403	Ferromagnetic	0.0444	Superparamagnetic

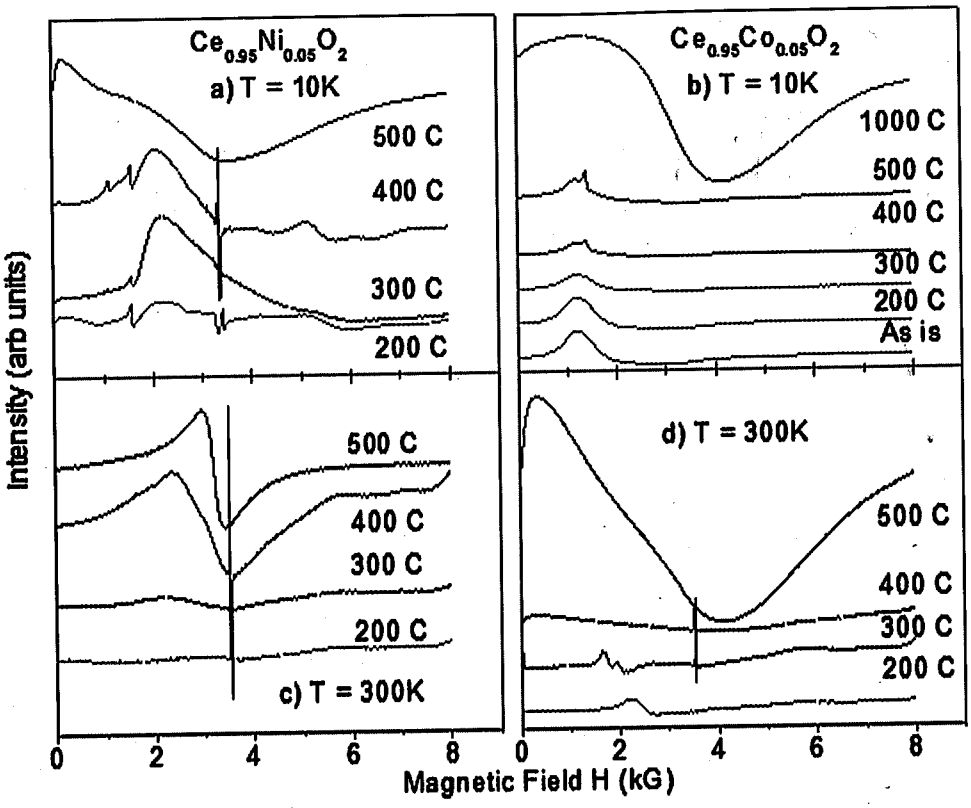

Fig. 3. Experimental EPR spectra of 5% Ni doped CeO_2 collected at (a) 10 K and (c) 300 K. Panels (b) and (d) show experimental EPR spectra of 5% Co doped CeO_2 collected at 10 K and 300 K, respectively. Labels show the annealing temperatures of the samples.

400 °C gradually decreases with increasing annealing temperature. However, for the sample annealed at 500 °C the magnetization increases by about two orders of magnitude, changing its nature from ferromagnetic to superparamagnetic. For higher annealing temperatures, diffusion of Ni ions toward the surface of the nanoparticles, as revealed by XPS studies, leads to surface enrichment with Ni ions, which leads to formation of antiferromagnetic NiO (T_N = 523 K).[19] This, in turn, causes a decrease of the saturation magnetization (M_s) of the samples annealed at 300 and 400 °C. However, the M_s of the sample annealed at 500 °C increases and it becomes superparamagnetic. It appears that the structure of nanoparticles for this sample changes considerably, because the oxygen loss, as revealed by the MS measurements, increases and the EPR spectrum due to the oxygen defects disappears completely. A more complex magnetic bonding of Ni ions might have formed here, such as a porous Ni/NiO bilayer clusters. *(b) Co.* The EPR spectra of 5% Co doped CeO_2 samples, shown in Figure 3(d), annealed at different temperatures exhibit rather complicated shapes. The samples, annealed at 400 and 500 °C, exhibit very broad ferromagnetic lines, which are consistent with the magnetization measurements. The EPR spectra of oxygen defects, exhibiting narrow, sharp lines, were also observed for the samples annealed at 300 and 400 °C. Two rather broad signals at $g = 3.46$ and $g = 4.05$ were observed in the sample annealed at 300 °C. These are most likely due to weak ferromagnetic

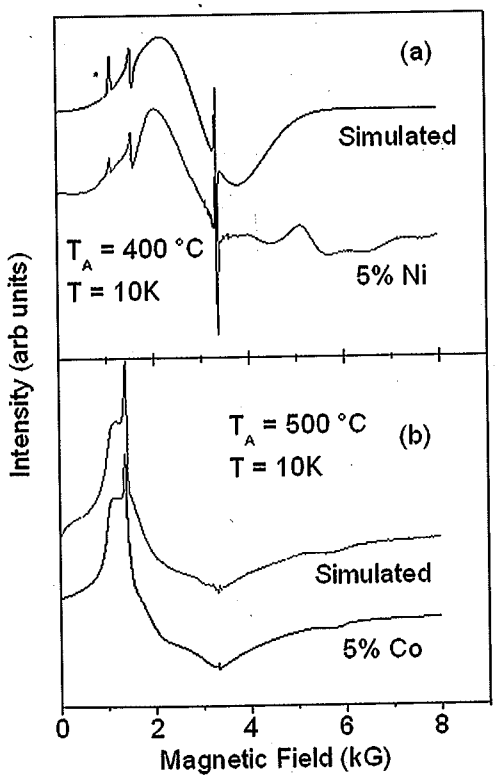

Fig. 4. Experimental and simulated EPR spectra of (a) 5% Ni-doped CeO_2 nanoparticles annealed at 500 °C and (b) 5% Co-doped CeO_2 nanoparticles annealed at 500 °C, both EPR spectra are collected at 10 K. The SH parameters used for simulation are listed in Table II.

states from two different kinds of CeO_2: Co nanoparticles, because paramagnetic signals from isolated Co ions cannot be detected at 300 K due to their rather short relaxation times, which broaden out the EPR lines completely. For the Co-doped samples, magnetization increases gradually with increasing annealing temperature; the increase in magnetization being the largest of all the samples for the sample annealed at 500 °C, exhibiting an intense FMR line.

3.4. Spin-Hamiltonian (SH) Parameters

In the present study there were observed two sets of EPR spectra corresponding to two different electronic spins, whose relevant SHs are described below.

$S = 1/2$ (low spin Co^{2+}): The following Spin Hamiltonian was used for the interpretation of EPR spectra

$$H_S = g_x\mu_B B_x S_x + g_y\mu_B B_y S_y + g_z\mu_B B_z S_z + A_x I_x S_x + A_y I_y S_y + A_z I_z S_z \quad (1)$$

Here, μ_B is the Bohr magneton, $i = x, y, z$, g_i are the principal values of the g-matrix, A_i are the principal values of the A-matrix, B_i are the components of the external magnetic field, S_i are the components of the electronic spin ($S = 1/2$), I_i the components of the nuclear spin of ^{59}Co ($I = 7/2$).

$S = 1$ (Ni^{2+}), one should add the higher order terms:

$$D[S_z^2 - (1/3)S(S+1)] + E[S_x^2 - S_y^2] \quad (2)$$

to the SH given by Eq. (1). Here D is the axial crystal-field parameter and E is the rhombic crystal-field parameter. The values of the various SH parameters used for fitting the EPR spectra considered here are listed in Table II below.

The Co^{2+} EPR spectra in CeO_2 observed here, characterized by a highly asymmetric g-matrix, at 4 and 10 K are similar to those observed in the Co-doped nanoparticles of SnO_2 at 5 K,[20] where they were ascribed to the Co ions in interstitial positions because of the very high anisotropy of their g-matrices. On the other hand, Co^{2+} ions in TiO_2, are characterized by highly anisotropic g and A matrices. This is due to the fact that there occurs a fairly large charge transfer to the surrounding ions, when doubly ionized Co^{2+} ions substitute for quadruply ionized Ti^{4+} ions.[21] Strong anisotropy in the components of g and A matrices then arises due to strong spin-orbital coupling, along with charge transfer to surrounding ions.[22] In an octahedral crystal field, which is prevalent in CeO_2, possessing cubic fluorite-like structure with 8-coordinated Ce ions, the lowest electron triplet ^4F becomes split, resulting in a doublet ground state,[22,23] with the effective spin $S = 1/2$. Distribution of crystal fields at Co^{2+} sites in nanoparticles leads to distribution in the g-values and, consequently, to broadening of EPR lines. This is reflected in broad individual lines of Co^{2+}, as verified by the present simulation of EPR spectra.

Two Co^{2+} EPR spectra, associated with spins $S = 1/2$ and 1, were also found in ZnO nanoparticles doped with

Table II. Parameters of experimental EPR spectra of Ni and Co ions in CeO_2 nanoparticles. The g-values and linewidths used for simulation of experimental spectra of 10 K EPR spectra of Co in CeO_2, annealed at 400 °C, and Ni in CeO_2, annealed at 400 °C, have been listed here. The values of the zero-filed splitting parameters D and E for Ni^{2+}, as well as the hyperfine parameters for Co^{2+} are listed in the footnotes.

Magnetic specie	Annealing temperature T_A (°C)	T (K)	Principal values of g-matrix			Linewidth (G)			Magnetic state
			g_x	g_y	g_z	ΔB_x	ΔB_y	ΔB_z	
Ni ions	200, 300, 400	10	2.25	2.25	2.25	1600	1600	1600	Ferromagnetic
Ni^{2+}	200, 300, 400	10	2.0	4.26	5.96	20	20	20	Paramagnetic
Ni ions	500	10	2.5	2.5	2.5	1800	1800	1800	Ferromagnetic
O^-	300, 400	10	2.0	2.0	2.0	10	10	10	Paramagnetic
$^{**}Co^{2+}$	200–500	10	1.17	3.6	5.4	80	400	80	Paramagnetic
$^{**}Co^{2+}$	400, 500	10	2.0	2.15	4.83	400	400	8	Paramagnetic
Co ions	200, 300, 400	10	4.3	4.3	4.3	800	800	800	Ferromagnetic
Co ions	1000	10	2.8	2.8	2.8	2000	2000	2000	Ferromagnetic
$^{*}Ni^{2+}$	200	300	2.06	2.06	2.22	95	95	450	Paramagnetic
Ni ions	200	300	2.1	2.1	2.1	1000	1000	1000	Ferromagnetic
Ni (1)	300	300	2.1	2.1	2.1	300	300	300	Superparamagnetic (15%)
Ni (2)	300	300	2.45	2.45	2.45	1220	1220	1220	Ferromagnetic (85%)
Ni (1)	400	300	2.2	2.2	2.2	450	450	450	Superparamagnetic (13%)
Ni (2)	400	300	2.35	2.35	2.35	1000	1000	1000	Ferromagnetic (87%)
Ni (1)	500	300	2.2	2.2	2.2	450	450	450	Superparamagnetic (95%)
O^-	300, 400	300	2.0	2.0	2.0	15	15	15	Paramagnetic
Co ions	200	300	2.86	2.86	2.86	420	420	420	Weak ferromagnetic
Co (1)	300	300	3.46	3.46	3.46	235	235	235	Weak ferromagnetic
Co (2)	300	300	4.05	4.05	4.05	187	187	187	Weak ferromagnetic
Co ions	400	300	3.2	3.2	3.2	3800	3800	3800	Ferromagnetic
Co ions	500	300	3.15	3.15	3.15	3750	3750	3750	Ferromagnetic

Notes: *Higher order SH parameters: for Ni^{2+} ($S = 1$): $D = 50$ G and $E = 0$ G; **Hyperfine (HF) parameters for Co^{2+} (1) ($I = 7/2$) – Co^{2+} (1): A_x, A_y, $A_z = 60$ G, 60 G, 60 G; Co^{2+}(2): A_x, A_y, $A_z = 7$ G, 7 G, 7 G.

Co ions,[24] similar to the ones presented here, observing two broad low-field lines ($g = 5$, $g = 3$) and a narrow line near $g = 4.5$. Here, the broad lines are interpreted to be due to to the core Co ions, and the narrow line due to the surface Co ions. The narrow line is due to Co^{2+} ions seeing tetragonal symmetry. It is is ascribed to the core Co ions, because there is not observed such a spectrum in the samples annealed at 200 °C, which are smallest in size ($R =$ 2.7 nm), and therefore possess virtually no core. When the annealing temperature increases, the size of nanoparticles increases, and a core is ultimately developed.

3.5. Magnetization

It is noted that no intense EPR line ascribed to O^- vacancies, near $g = 2.0$, was observed, for the samples annealed at 300° and 400 °C. Furthermore, this signal is completely suppressed in smaller samples, produced by annealing at 200 °C. The intensity of this signal due to O^{-2} vacancies increases with higher annealing temperature, because the core part of nanoparticles becomes more uniform in larger samples. And, finally, at the highest annealing temperature (500 °C), all oxygen vacancies participate in ferromagnetic ordering due to the FCE (F-centers exchange) mechanism.[25] As mentioned above for Co-doped CeO_2 sample, Co ions diffuse toward the core with increasing annealing temperature, where the concentration of oxygen vacancies is high. As a consequence the saturation magnetization increases with increasing annealing temperature. Contrary to this, in Ni-doped CeO_2, Ni ions diffuse outward to the surface with increasing annealing temperature, causing the saturation magnetization to decrease with increasing annealing temperature to 400 °C. The saturation magnetization increases above 400 °C due to manifestation of superparamagnetism. Finally, at the highest annealing temperature (500 °C), ferromagnetism disappears, giving rise to superparamagnetism, as a consequence of large particle size. Separation of core volume from surface area takes place as the particle size increases with increasing annealing temperature. This leads to different behaviors: ferromagnetic and superparamagnetic for the surface and core regions, respectively. In the core, superparamagnetic clusters of Co-□-Co are formed, which are not bonded, where denotes the oxygen vacancy, to each other, so that percolation network does not extend over the entire nanoparticle, due to breakdown of ferromagnetic network into separate disconnected magnetic clusters. This is caused by the fact that the nanoparticles, annealed at the low temperature of 200 °C have a small average size of 2.7 nm, which is rather small and quite homogeneous. Then, the average number of oxygen vacancies on the surface and those in the core volume are not much different from each other. When the annealing temperature is increased, the nanoparticle size increases, and the average number of oxygen vacancies on the surface and those in the core volume become different from each other. The surface area becomes enriched with oxygen vacancies; as a consequence, the ferromagnetic network manifests on the surface. The core volume, on the other hand, becomes depleted in oxygen vacancies, experiencing a breakdown of ferromagnetic network, resulting in physically separate magnetic clusters, each exhibiting superparamagnetic behavior.

3.6. Mechanism of Ferromagnetism in Co- and Ni-Doped CeO_2

There are several models proposed in the literature to explain ferromagnetism in these samples.

(i) & (ii) One possible origin of the observed ferromagnetism in dilute magnetic semiconductors (DMS) is the interaction between the doped paramagnetic ions via charge carriers invoking exchange interaction, as proposed by Dietl et al.[26] in the modified Zener model.[27]

(ii) Another model for occurrence of intrinsic ferromagnetism in DMS is related to the exchange of impurity ions via F centers,[25,26] involving the superexchange interaction between the complexes formed by the impurity ions and oxygen vacancies.[28] Oxygen vacancies, as well as cerium vacancies, concentrate on the surface of nanoparticle and electroneutrality in this area is secured by charge compensation of Ce^{4+} vacancy and two O^{2-} vacancies. Oxygen vacancies in core area appear only due to charge compensation of transition metal impurities ions, i.e., Ni^{2+}. Recently, leading role of oxygen vacancies on ferromagnetic properties of oxide nanoparticles was proved directly by irradiation of these nanoparticles and related calculations.[29] Formation of oxygen vacancies, and, consequently, magnetic F-centers, depends strongly on the method of synthesis, surface properties and doping effects as pointed out recently by Alanko et al.[30] Thus, the occurrence of room-temperature ferromagnetism depends on

(a) the concentration of oxygen vacancies, located mainly at the surface of nanoparticles,
(b) numbers of impurity transition metal ions, and
(c) charge-carrier density.

Vinokurov et al.[31,32] found, from their investigations of conductivity and oxygen diffusion in bulk CeO_2, that in oxidized samples, wherein the oxygen defects have been suppressed, the annealed samples possess very different conductivities. The TGA-MS data presented here clearly indicate that for annealing temperatures $T_A \geq 300$ °C, there is a gradual increase in released oxygen with increasing T_A, indicating that oxygen vacancies increase with annealing temperature. Thus, increasing T_A enhances ferromagnetism in doped CeO_2 samples due to change in the number of charge carriers and their activation properties. Presence of transition-metal ions and their local structure/environments also play important roles, so that at room temperature the. CeO_2 sample, doped with Ni ions,

prepared at the highest annealing temperature, is found to be superparamagnetic, whereas CeO_2 samples doped only with Co ions are found to be ferromagnetic.

(iii) Yet another potential origin for the observed ferromagnetic behavior is the possible presence of metal (Co or Ni) clusters in the annealed samples, as suggested in Refs. [13–15]. This is supported by the MS data, which indicate that the samples undergo continued oxygen loss as the annealing temperature increases, producing at the same time, metallic nanoparticles that are ferromagnetic or superparamagnetic depending on their size.

(vi) Presence of metallic clusters of Co ions is also an origin of intrinsic ferromagnetism of CeO_2 nanoparticles, doped with Co ions. Following recent research,[33] Co ions usually form the clusters in magnetic oxide semiconductor particles without the surfactant.

3.7. Coexistence of Ferromagnetic and Paramagnetic Phases in Co- and Ni-Doped CeO_2

It can be explained on the basis of FCE (F-center exchange) model of ferromagnetism,[25] mentioned above. The broad ferromagnetic line observed in the CeO_2 samples, annealed at 400 and 500 °C, as recorded at 4.10 K, is most likely related to the intrinsic ferromagnetism of Co ions, which interact through the magnetic F-color centers (oxygen vacancies), which trap electrons.[34] Accordingly, there exist some regions in the sample with increased density of oxygen vacancies, which produces a ferromagnetically coupled network over the entire region, consisting of Co^{2+}-□-Co^{2+} groups, where □ denotes the oxygen vacancy, exhibiting a ferromagnetic signal. The complex magnetic behavior of Co-doped CeO_2 can be explained to be due to the competition of super-exchange coupling, which leads to antiferromagnetic ordering, whereas the FCE coupling leads to ferromagnetic ordering. In the regions, which lack such oxygen vacancies, the Co ions there are not bound together through magnetic color centers. These isolated Co ions then give rise to a paramagnetic signal. Consequently, there occurs coexistence of paramagnetic and ferromagnetic signals in CeO_2 nanoparticles. This model was successfully applied to Co-doped CeO_2.[9] The influence of oxygen vacancies in producing ferromagnetism was carefully investigated in Co-doped CeO_2 samples,[7,8] as well as in undoped CeO_2 samples.[35] The same model can be applied to understand ferromagnetism in Ni-doped CeO_2. It was found that the strength of magnetization due to F-centers in CeO_2, related to the number of F-centers present, depends strongly on the annealing temperature.[36] Consequently, these centers do not only serve as media in FCE coupling, leading to ferromagnetism, but they also modify the magnetization of the paramagnetic regions in CeO_2 nanoparticles strongly.

4. CONCLUDING REMARKS

The salient features of the present study are as follows.

(i) The FMR/EPR data on the investigated CeO_2 samples are fully consistent with their magnetic measurements. They provide a good understanding of both the magnetism of the isolated ions and ferromagnetism due to exchanged-coupled ions that exist in the samples.

(ii) EPR and TGA-MS data provide evidence for increased formation of oxygen vacancies as the annealing temperature, T_A, increases. This plays a major role in the magnetic properties of the annealed samples.

(iii) Different behaviors of saturation magnetization in the samples doped with Co ions as compared to those with Ni ions, from 200 to 400 °C, is interpreted to be due to different—toward and outward surface diffusions, respectively, of these impurity ions during annealing.

(iv) A simulation of EPR/FMR spectra of isolated Co and Ni ions carried out here provides more details on the spins and the corresponding SH parameters for the transitions metal ions Ni and Co present in the samples. This, in turn, helps to understand the role of the doped ions and oxygen (O^-) vacancies on the observed magnetic properties.

(v) The various mechanisms of occurrence of ferromagnetism in Co- and Ni-doped CeO_2, as well as coexistence of ferromagnetic and paramagnetic phases in these samples have been discussed.

(vi) A model for the formation of superparamagnetic state in the sample of CeO_2, doped with 5% Ni, has been proposed here.

Acknowledgments: SKM is grateful to the Natural Sciences and Engineering Research Council of Canada (NSERC) for partial financial support. Research at Boise State University was supported by NSF-CAREER program (DMR-0449639), NSF-RUI (DMR-0840227), DoE-EPSCoR program (DE-FG02-04ER46142), ARO grant (W911NF-09-1-0051), and at Northwest Nazarene University by NSF-RUI (DMR-0840265) and SIA is grateful to the project RNP-31 of Ministry of Education of Russian Federation.

References and Notes

1. H. S. Nalwa (ed.), Magnetic Nanostructures, 2nd edn., American Scientific Publishers, Los Angeles (**2009**).
2. A. Thurber, K. M. Reddy, and A. Punnoose, *J. App. Phys.* 101, 09N506 (**2007**).
3. A. Thurber, K. M. Reddy, V. Shutthanandan, M. H. Engelhard, C. Wang, J. Hays, and A. Punnoose, *Phys. Rev. B* , 76, 165206 (**2007**).
4. S. Kumar, Y. J. Kim, B. H. Koo, and C. G. Lee, *J. Nanosci. Nanotechnol.* 10, 7204 (**2010**).
5. A. Tiwari, V. M. Bhosle, S. Ramachandran, N. Sudhakar, J. Narayan, S. Budak, and A. Gupta, *Appl. Phys. Lett.* 88, 142511 (**2006**).
6. Y. Q. Song, Q. H. Yang, H. W. Zhang, L. Peng, and L. R. Shah, *J. Phys.: Conf. Ser.* 152, 012038 (**2009**).

RESEARCH ARTICLE

7. Y.-Q. Song, H.-W. Zhang, Q.-Y. Wen, L. Peng, and J. Q. Xiao, *J. Phys.: Condensed Matter.* 20, 255210 **(2008)**.
8. L. R. Shah, B. Ali, H. Zhu, W. G. Wang, Y. Q. Song, H. W. Zhang, S. I. Shah, and J. Q. Xiao, *J. Phys: Condens. Matter* 21, 486004 **(2009)**.
9. Q.-Y. Wen, H.-W. Zhang, Y.-Q. Song, Q.-H. Yang, H. Zhu, and J. Q. Xiao, *J. Phys.: Condens. Matter.* 19, 246205 **(2007)**.
10. B. Vodungbo, F. Vidal, Y. Zheng, M. Marangolo, D. Demaille, V. H. Etgens, J. Varalda, A. J. A. de Oliveira, F. Maccherozzi, and G. Panaccione, *J. Phys.: Condens. Matter* 20, 125222 **(2008)**.
11. V. Fernandes, J. J. Klein, N. Mattoso, D. H. Mosca, E. Silveira, E. Ribeiro, W. H. Schreiner, J. Varalda, and A. J. A. de Oliveira, *Phys. Rev. B* 75, 121304(R) **(2007)**.
12. B. Vodungbo, Y. Zheng, F. Vidal, D. Demaille, V. H. Etgens, and D. H. Mosca, *Appl. Phys. Lett.* 90, 062510 **(2007)**.
13. S. Colis, A. Bouaine, R. Moubah, G. Schmerber, C. Ulhaq-Bouillet, A. Dinia, L. Dahéron, J. Petersen, and C. Becker, *J. App. Phys.* 108, 053910 **(2010)**.
14. A. Bouaine, R. J. Green, S. Colis, P. Bazylewski, G. S. Chang, A. Moewes, E. Z. Kurmaev, and A. Dinia, *J. Phys. Chem. C* 115, 1556 **(2011)**.
15. S. Colis, A. Bouaine, G. Schmerber, C. Ulhaq-Bouillet, A. Dinia, S. Choua, and P. Turek, *Phys. Chem. Chem. Phys.* 14, 7256 **(2012)**.
16. S. K. Misra, S. I. Andronenko, M. E. Engelhard, A. Thurber, K. M. Reddy, and A. Punnoose, *J. App. Phys.* 103, 07D122 **(2008)**.
17. N. Jedrecy, H. J. von Bardeleben, Y. Zheng, and J. L. Cantin, *Phys. Rev. B* 69, 041308 **(2004)**.
18. S. V. Chong, K. Kadowaki, J. Xia, and H. Idriss, *Appl. Phys. Lett.* 92, 232502 **(2008)**.
19. M. Jagodič, Z. Jagličić, A. Jelen, J. B. Lee, Y.-M. Kim, H. J. Kim, and J. Dolinšek, *J. Phys.: Condens. Matter* 21, 215302 **(2009)**.
20. S. K. Misra, S. I. Andronenko, K. M. Reddy, J. Hays, and A. Punnoose, *J. App. Phys.* 99, 08M106 **(2006)**.
21. E. Yamaka and R. G. Barnes, *Phys. Rev.* 125, 1568 **(1962)**.
22. A. Abragam and B. Bleaney, Electron Paramagnetic Resonance of Transition Ions, Clarendon, Oxford **(1970)**.
23. M. J. R. Hoch, S. Nellutla, J. van Tol, E. S. Choi, J. Lu, and H. Zheng, J. F. Mitchell, *Phys. Rev. B* 79, 214421 **(2009)**.
24. P. Lommens, F. Loncke, P. F. Smet, F. Callens, D. Poelman, H. Vrielinck, and Z. Hens, *Chem. Mater.* 19, 5576 **(2007)**.
25. J. M. D. Coey, M. Venkatesan, and C. B. Fitzgerald, *Nat. Mater.* 4, 173 **(2005)**.
26. T. Dietl, H. Ohno, F. Matsukura, J. Cibert, and D. Ferrand, *Science* 287, 1019 **(2000)**.
27. C. Zener, *Phys. Rev.* 82, 403 **(1951)**.
28. K. Kikoin and V. Fleurov, *Phys. Rev. B*, 74, 174407 **(2006)**.
29. A. A. Achkeev, I. R. Vakhitov, R. I. Khaibullin, and L. R. Tagirov, *J.Phys.: Conf. Ser.* 394, 012018 **(2012)**.
30. G. A. Alanko, A. Thurber, Ch. Hanna, and A. Punnoose, *J. App Phys.* 111, 07C321 **(2012)**.
31. I. V. Vinokurov, Z. N. Zonn, and V. A. Ioffe, *Sov. Phys.-Solid St.* 9, 2659 **(1968)**.
32. I. V. Vinokurov and V. A. Ioffe, *Sov. Phys.-Solid. State* 11, 207 **(1969)**.
33. H. Jiang, X. F. Lio, Z. Y. Zou, R. H. Tang, W. Lio, and R. H. Yu, *J. Nanosci. Nanotechnol.* 13, 1111 **(2013)**.
34. J. M. D. Coey, A. P. Douvalls, C. B. Fitzgerald, and M. Venkatesan, *Appl. Phys. Lett.* 84, 13332 **(2004)**.
35. S.-Y. Chen, Y.-H. Lu, T.-W. Huang, D.-C. Yan, and C.-L. Dong, *J. Phys. Chem. C* 114, 19576 **(2010)**.
36. V. E. Adamyan, I. V. Vinokurov, N. A. Mantashyan, and S. V. Stepanyan, *Sov. Phys.-Solid. State* 13, 1934 **(1972)**.

Received: 15 March 2013. Accepted: 6 April 2013.